

B. Boron profile

The boron profile generated by these implants was evaluated with SIMS. The profiles for the same samples whose TEM images are in Figure 1 are shown in Figure 2. While it was expected that the profiles would overlap, it is observed that the B36 profile is slightly deeper than the B18. This surprising observation lead to an extensive study of the profile of B36 as a function of dose and energy. The deeper profile was observed at 1E15 and higher doses, with the degree of increased depth increasing with dose. The analysis of this profile effect is that there is a knock-on mechanism which drives some of the already implanted boron slightly deeper, with the effect observable above 5E14 dose and increasing as the boron concentration increases. It is shown in Figure 2 that the increase in junction depth for B36 is about 1nm compared to B18. This figure also shows the SIMS profile difference for PCOR and HDR SIMS protocols. The PCOR profile shows a significantly deeper profile than the HDR. The HDR profile agrees well with TRIM simulations of the process conditions used. It is important to use the appropriate SIMS methodology for the process space being evaluated.

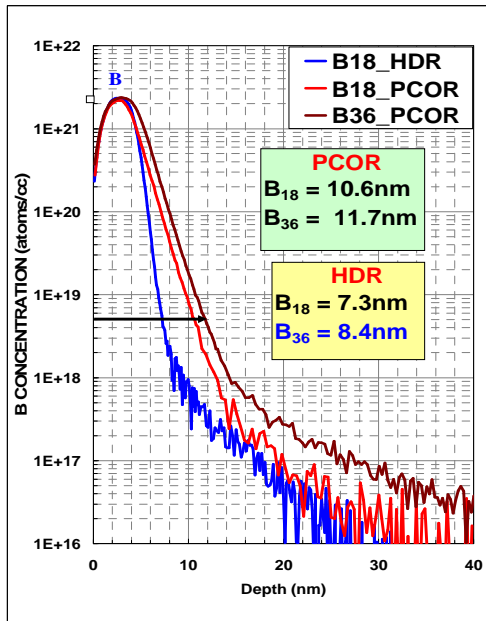


Figure 2: SIMS profiles for B36 and B18 implants of 1E15 dose and 300eV equivalent.

C. Boron activation

One of the key advantages of molecular

implantation in general is high activation after annealing. The most direct means of evaluating activation levels is to measure the sheet resistance, R_s , of the junctions being formed.

For this study, samples have been annealed using the Excico excimer laser annealing system. The excimer laser pulses are about 150ns duration. The laser powers used were specifically chosen to prevent melting of the silicon surface. The energy range was 1.35-1.45J/cm² per pulse. The Excico system is a stepper-type system with the option of multiple pulses at each site prior to stepping. The experiments included tests of one, five and ten pulses. With such a short anneal time, this is a true diffusion-less anneal. Some of the resulting R_s data is shown in Figure 3. For this experiment, the implant dose was 9E14/cm² and the implant energy was 300eV equivalent. It is observed that the B18 and B36 samples have the same response to the laser pulse energy and number of pulses. But, the B36 values of R_s are all dramatically lower (better) than the B18 values. While the B36 profiles are slightly deeper, as noted, this is not enough to explain the remarkable improvement in R_s shown by B36. Since these junctions are approximately 10nm deep, achieving an R_s below 1000 ohm/sq is very challenging; the B18 results are better than most reports with conventional implant. The B36 R_s numbers are consistent with an activation level of around 1.8E20/cm².

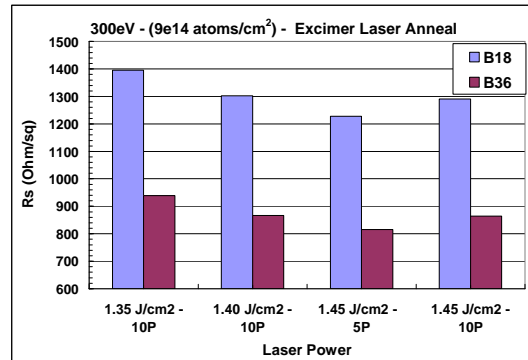


Figure 3: Sheet resistance vs. laser power and number of pulses, B18 and B36.

D. B36 activation

The very low R_s numbers observed with B36 compared to B18 require explanation. It is not due to interaction with the excimer laser anneal since the same trend and similar numbers have been seen with other annealing methods. The analysis connects the low R_s numbers with the deeper amorphous layers created with B36. To show this effect, a model is

presented in Figure 4. This figure shows the amount of boron contained in a layer of any thickness as a percentage of the total boron in the implant. This model has been generated by integrating the SIMS profile from the surface to any given depth and normalizing to the total dose. Further, it has been assumed that the activation level is at most $2.5E20/cm^2$, so the integration is capped at this value. Next, it is assumed that only boron in the amorphous layer is activated. It was shown above that the amorphous layer thickness for B18 and B36 were 5.0 and 6.3nm respectively. Comparing the corresponding values in Figure 4 it is observed that about 85% of the boron is in the amorphous layer for B18 but 98% is in the amorphous layer for B36. This is the mechanism for higher levels of activation observed with B36 implantation. If you include the lost boron in the native oxide, the percentage increase with B36 is even greater.

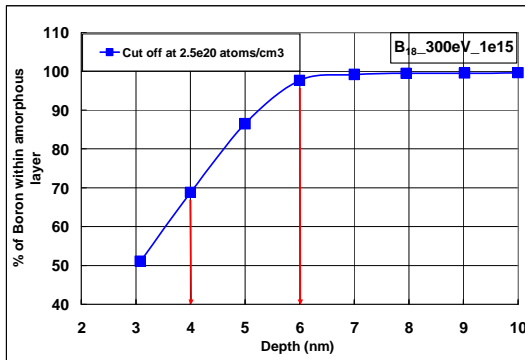


Figure 4: A model for the percentage of boron contained in an amorphous layer of a given thickness.

In summary, it has been shown that the use of the dimer of ClusterBoron, or B36, has significant advantages for ultra-low energy implantation. B36 produces a deeper amorphous layer than B18, which results in a dramatic improvement of the sheet resistance. While the profile is seen to be slightly deeper at high doses, the dose required for the SDE implant will likely be moderate, and thereby minimize the impact of the knock-on mechanism. Overall, it is found that the use of B36 is very beneficial for implants below 400eV.

3. ClusterCarbon

Molecular implantation with hydrocarbon molecules is also rapidly gaining acceptance across the industry. Most of the early work with carbon molecules has been directed at the PAI and diffusion control applications [3]. These processes have been

well developed and will not be discussed here. The features of ClusterCarbon make it an attractive approach to generating a Si:C stress layer for NMOS device enhancement. The ClusterCarbon development to be discussed here will be directed at the stressor application [4].

A. Carbon molecule species

For the PAI and diffusion control applications, the carbon molecule generally used is $C_{16}H_{10}$ but this species has a maximum energy limitation, so its application to the stress process is limited. The carbon source material used to get higher energy implant process, and thus deeper stressor layers is $C_{14}H_{14}$. The mass spectrum observed using this source material is shown in Figure 5. While the parent species is observed, and so available for implantation, it is clear that the highest intensity beam from this material is C7. With an 80kV maximum operating voltage, the C7 molecule allows a process energy up to about 11keV carbon equivalent. Using the doses appropriate to achieve about 1.5% atomic concentration, the resulting amorphous layer, and thus stressor layer thickness is around 40nm. While this has been shown to be useful for integration into a CMOS process flow and achieving stress enhancement to the devices, some integration schemes would prefer a deeper carbon implant and a thicker stressor layer.

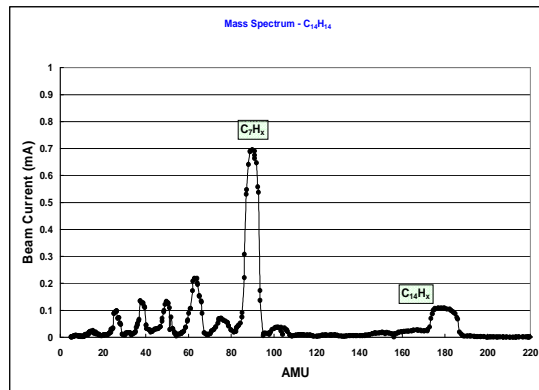


Figure 5: The mass spectrum resulting with $C_{14}H_{14}$ source material.

To achieve a thicker stressor layer with a fixed extraction voltage limit requires going to a smaller molecule. In Figure 5, it is seen that there is a beam available with peak intensity in the low 60s AMU which is the C_5H_5 fraction of the $C_{14}H_{14}$ parent. Use of this species will allow carbon equivalent energies of up to 14keV to be implanted. Early work with this specie showed that implants of only C5 had significantly less amorphization than C7, but lately a

multiple implant scheme has been developed to achieve a carbon profile in depth which is flat. Thus, it is possible to add a higher energy C5 implant to a multiple C7 sequence to attempt to extend the amorphous thickness depth. The result of such an experiment is shown in Figure 6. This figure shows the simple case of a single C7 implant at 10keV equivalent and the same implant with the addition of a C5 implant at 14keV. The TEM images show that the amorphous layer has been increased from 36.5nm to 53nm by the addition of the C5 implant. Further experimentation has shown the ability to achieve stressor layers of 60nm or more using this approach.

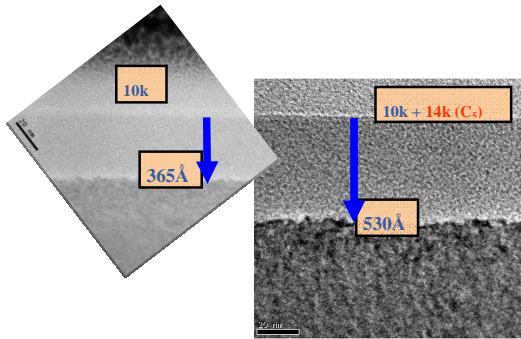


Figure 6: TEM images showing the increase of amorphous layer thickness by adding a C5 implant

B. Carbon and phosphorus interaction

It has been shown to be very straightforward to perform carbon implantation and achieve Si:C layers that produce high values of stress. Most of the time these layers are not compatible with simultaneously forming a good junction. There is direct competition between the carbon and dopant atoms for substitutional sites and the presence of both types of impurity complicates both the stress and junction processes. In particular, the high concentrations of carbon required to form the very aggressive stress layers make it very difficult to activate the phosphorus dopant. An example of this interaction is shown in Figure 7. This figure shows the phosphorus sheet resistance as the carbon concentration is increased. It is observed that any carbon increases the sheet resistance and the rate of increase accelerates as the carbon concentration increases. It is noted that the carbon equilibrium solubility is around 1.6%. Carbon atomic concentrations above this level cannot possibly achieve 100% substitutionality, so such layers contain much excess carbon which readily interacts with the phosphorus, resulting in de-activation.

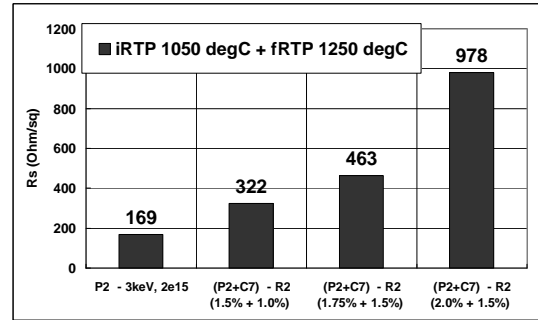


Figure 7: Sheet resistance of the phosphorus junction as the carbon concentration is increased.

Further evidence of this direct interaction is seen in the anneal dependences. In Figure 8 the dependence of the phosphorus sheet resistance vs. anneal process is shown. The anneal options are flash anneal at 1200C with or without spike anneal at 1000C or 1050C. The flash only samples have the highest sheet resistance with higher spike anneal temp producing lower Rs value.

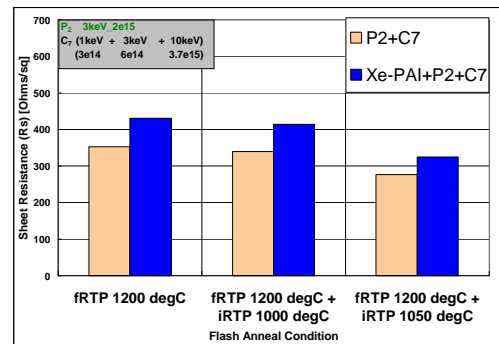


Figure 7: Sheet resistance values vs anneal process.

However, the carbon substitutionality is also affected by the anneal process. Figure 8 shows the carbon substitutional fraction as a function of anneal process. It is seen that the substitutional carbon declines exactly as the phosphorus substitutional (active) fraction increases.

The trends shown in these data guide the development path, within many other constraints. The best net results will be achieved when moderate processes are used for both carbon and dopants. Carbon concentration above the equilibrium solubility (1.6%) produce interstitial carbon which aggressively deactivates the dopant atoms. Similarly, dopant processes which introduce excessive dopant beyond what can be activated, which most conventional junction processes do, will make it very difficult to

achieve high carbon substitutionality. Both carbon and dopant results are very dependent on the annealing technology used. The optimum window is moderation with all processes, with ms anneal and no high temperature spike.

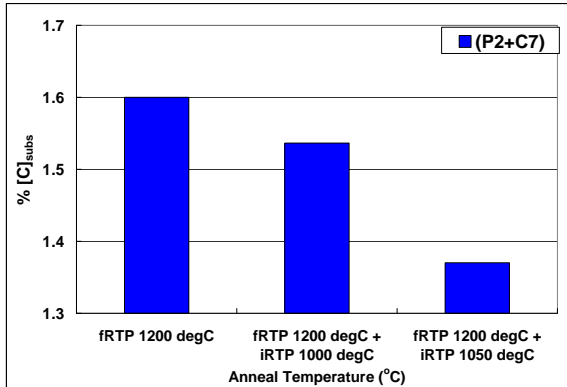


Figure 8: Carbon substitutional fraction as a function of anneal process.

4. Conclusions and Summary

Molecular implantation has special features which directly result from the cluster nature of the implant process. These features have been shown to be directly responsible for the advantageous process results available from molecular implant. The use of the dimer of ClusterBoron has been shown to produce very highly active, extremely shallow junctions. The use of the C5 molecule is shown to expand the range of stressor layer thicknesses available. Analysis of the interaction between carbon and dopant atoms drives the optimization process to moderate concentrations of both impurities. Molecular or cluster implant is shown to be essential to the most advanced implant applications in today's developments.

Acknowledgments

The author thanks Dr. K. Sekar for all his efforts. Thanks also to Excico and Mattson for annealing technology.

References

- [1]. W. Krull, B. Haslam, T. Horsky, T. Verheyden and K. Funk, Proc. Of International Conf. on IIT (2006) p 142.
- [2]. K. Sekar, W. Krull, T. Horsky, D. Jacobson, K. Jones, and D. Henke, Proc. Of the International Conf on INSIGHT in Semiconductor Device Fabrication, Metrology, and Modeling (2007) p 141.
- [3]. A. Cacciato, et al., J. Appl. Phys. 79 (1996) p 2314.
- [4]. K. Sekar, et al., Materials Science and Eng. B 154-155, (2008) p122.